Detection of Long and Short DNA Using Nanopores with Graphitic Polyhedral Edges

Kevin J. Freedman,[†] Chi Won Ahn,[‡] and Min Jun Kim[§,*]

[†]Department of Chemical and Biological Engineering, Drexel University, Philadelphia, Pennsylvania 19104, United States, [‡]Nano-Materials Laboratory, National Nanofab Center, Daejeon, Korea 305-806, and [§]Department of Mechanical Engineering and Mechanics, Drexel University, Philadelphia, Pennsylvania 19104, United States

ABSTRACT Graphene is a unique material with a thickness as low as a single atom, high in-plane conductivity and a robust lattice that is self-supporting over large length scales. Schematically, graphene is an ideal solid-state material for tuning the properties of a nanopore because self-supported sheets, ranging from single to multiple atomic layers, can create pores with near-arbitrary dimensions which can provide exquisite control of the electric field drop within the pore. In this study, we characterize the drilling kinetics of nanopores using a thermionic electron source and various electron beam fluxes to minimize secondary hole formation. Once established, we investigated the use of multilayer graphene to create highly tailored nanostructures including nanopores with graphite polyhedral crystals formed around the nanopore edge. Finally, we report on the translocation of double stranded and single stranded DNA through such graphene pores and show that the single stranded DNA translocates much slower allowing detection of extremely short fragments (25 nucleotides in length). Our findings suggest that the kinetic and controllable properties of graphene nanopores under sculpting conditions can be used to further enhance the detection of DNA analytes.

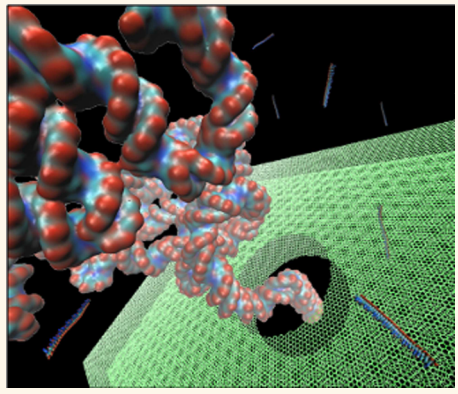

KEYWORDS: graphene · nanopore · DNA sequencing · graphite polyhedral crystals

Using an electric field to drive molecules through a nanoscale pore for bioanalytical analysis has become a widely used method to study single molecule kinetics and behavior.[1−5] The proposed utility of nanopore-based devices range from commercial applications, such as ultrafast DNA sequencing[2,6] and protein molecular recognition,[7,8] to answering fundamental questions regarding single molecule biophysics.[1,9,10] A majority of experiments drive molecules through an ultrathin membrane containing a single pore allowing one to detect a transient decrease in the flow of ionic current, and therefore an increase in electrical resistance.[6] Traditionally, solid-state pores are fabricated within silicon nitride thin films typically between 20 and 50 nm,[1,11−13] while electron beam lithography has been shown to thin regions of the membrane to even lower membrane thicknesses reaching sub-10 nm and thereby enhancing the resolution of nanopore sensing.[14] To achieve even thinner membranes, graphene has been proposed to be an ideal candidate for next generation nanopore devices.[15−17]

Graphene is defined as a single atomic layer of sp^2-bonded carbon atoms and is the fundamental structural element of many interesting nanostructures; namely carbon nanotubes, fullerenes, and nanoribbons. Additional novel structures have been created that combine the unique electrical and mechanical properties of graphene with other thin film structures such as cantilevers,[18] nanoelectrodes,[19] and nanopores.[15−17] For this purpose, single-layer and few-layer suspended graphene sheets have been of great interest and fabricated using a focused electron beam.[15−17,20] The inherent advantage of using an electron beam sculpting technique is that both fabrication and imaging can be performed in the same instrument allowing visual feedback of device progression. Although sculpting conditions (>140 kV) can introduce defects and cause amorphization of graphene,[20,21] methods such as annealing, current-induced graphitization,

* Address correspondence to mkim@coe.drexel.edu.

Received for review January 23, 2013 and accepted May 28, 2013.

Published online May 28, 2013
10.1021/nn4003665

or low-energy electron beam irradiation can reverse the process causing amorphous carbon to return to single or poly crystalline graphene.[22−25] Here we observe that drilling with low beam intensities in multilayer graphene preserves the graphene crystal structure, and further, electron beam conditions can be used to create novel graphitic structures around the edge of the nanopore.

The dominant instrument utilized for electron beam sculpting, particularly for nanopore fabrication, is a 200 kV field emission transmission electron microscope (TEM) whose field emission source provides the highest flux of electrons.[26,27] Thermionic sources have failed to drill in silicon nitride membranes, the most commonly used thin film, due to lower electron beam densities of the convergent beam. However, due to the thin nature of graphene, we explored the use of a thermionic source (lanthium hexaboride) in order to expose graphene to lower doses of electrons. Experiments were performed within a JEOL JEM 2100 TEM operated at 200 kV (with varying beam intensities) which was used to both sculpt and image graphene grown by chemical vapor deposition (CVD) method. The first reports of graphene nanopore drilling using an electron beam used field emission sources without using beam intensity to manipulate pore diameter. With the lower beam currents offered by the thermionic source, we aimed to characterize drill times to create reproducible pore sizes and minimize membrane damage, develop graphitic structures around the pore edge, and characterize the thickness and geometry of the pore using TEM tomography.

Despite offering several advantages to next-generation DNA sequencing which requires single stranded DNA as its primary analyte, previous reports have focused on proof-of-concept experiments using double stranded DNA.[15−17] The first proposed advantage of graphene over silicon nitride pores is its atomically thin structure allowing ultrahigh resolution sensing. Second, the graphene can be used as an electrically active material which can manipulate DNA movement or even measure the transverse conductance of each DNA base *via* tunneling.[15] Here we report on the fabrication of multilayer graphitic structures which are capable of offering new and highly advantageous properties to graphene nanopores. Since multilayer graphene structures can be tuned electrically[28] and geometrically[29] using its layers as a design parameter, graphene as a starting material is highly robust for single molecule sensing. To test the utility of the nanopores, DNA−pore interactions were studied using double stranded DNA and short single stranded DNA fragment 25 nucleotides in length. Through the detection of these short DNA fragments, we suggest that having a graphitic edge with a curved, yet planar, surface facing the inside of the pore is useful to future DNA sensing applications.

RESULTS AND DISCUSSION

Graphene Nanopores with Graphitic Edges: Fabrication and Characterization. The current densities of the convergent beam were controlled by spot settings alone and were varied within the range of 10^5-10^7 electrons/(nm$^2\cdot$s) which led to very different sculpting kinetics. Imaging with a less convergent beam was performed at 10^4-10^5 electrons/(nm$^2\cdot$s) leading to no obvious change in the appearance or physical properties of sculpted structures allowing one to stop drilling, image and continue drilling as necessary. The drilling was done in areas with single crystalline properties as measured by the diffraction pattern (Figure S4). By reducing the electron beam intensity, a slower rate of nanopore growth can be achieved allowing fine-tuning of the nanopore size (Figure 1). Assuming graphene is present, this method led to 100% yield rate for nanopores ranging from 1 to 140 nm in diameter (TEM image of 1.2 nm nanopore supplied in Supporting Information Figure S1). The use of different beam intensities was incredibly important in this study as we observed that each spot mode was ideal for fabricating a different range of nanopores. The highest beam intensity, which is most similar to the current densities used in previous studies (10^7 electrons/(nm$^2\cdot$s)),[26] was least ideal for creating pores smaller or greater than its beam size and led to peripheral holes around the main nanopore and/or jagged edges as mentioned by others.[30,31] Qualitatively, 6×10^5 and 2×10^5 electrons/(nm$^2\cdot$s) produced optimal pores with no damage to the surrounding graphene membrane, while 6.8×10^6 and 2×10^6 electrons/(nm$^2\cdot$s) only rarely produced noticeable damage. TEM diffraction patterns were collected before and after drilling as well as over the course of

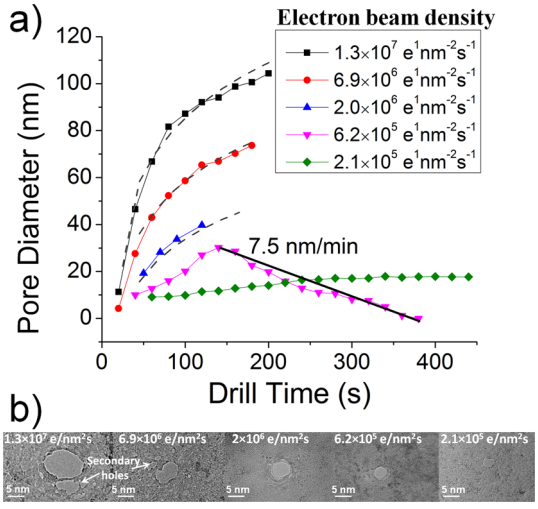

Figure 1. Drilling and shrinking kinetics of graphene nanopores using various beam intensities. (a) Pore kinetics as a function of beam residence time, or drill time (s) for 5 different beam intensities. (b) TEM images of initial pore formation using 5 different beam intensities resulting in varying degrees of edge damage around the pore.

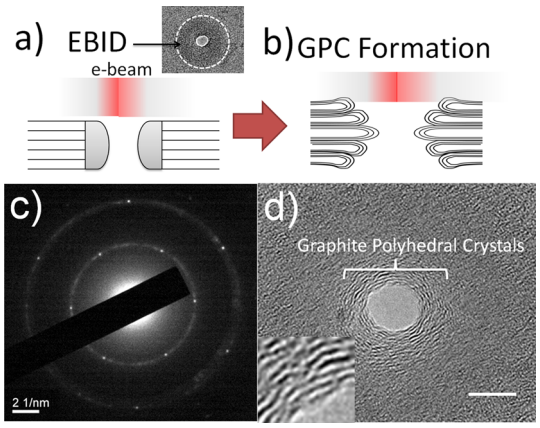

Figure 2. (a) A schematic illustrating the use of electron beam induced deposition (EBID) to cover the pore surface with amorphous carbon. (b) A schematic illustrating the use of the TEM electron beam to induce a transformation from amorphous carbon to graphitic polyhedral crystals (GPC). (c) Diffraction pattern of graphene irrespective of long-term TEM imaging showing single crystalline structure. Some areas displayed poly crystalline structure (Figure S4) but were avoided when drilling nanopores. (d) Shrunk nanopore with graphite polyhedral crystal edges sculpted at 6.2 $\times$ 10^5 electrons/(nm^2·s). Inset: close up of nanopore edge. Scale bar = 5 nm.

10−20 min and led to stable diffraction patterns (Figure 2c). The seeming lack of susceptibility of multilayer graphene to become amorphous carbon under electron beam irradiation is believed to be due to the lower atomic mobility of atoms when several graphene sheets are present to confine and minimize dislocations, particularly at lower electron beam densities.[32,33]

Electron beam induced deposition (EBID) of amorphous carbon onto graphene is commonly reported to be detrimental to nanopore fabrication due to the loss pristine graphene; however, evidence for diminished sensing ability or thickness variation of the membrane has not been thoroughly investigated.[20,31] Here, EBID was not observed with 4 out of the 5 beam intensities and was verified by a long-term drilling study in which the beam was focused to a spot for over 15 min (Figure S1). Most of the nanopore drilling kinetics produced well behaved logarithmic growth described by $D_p = AI_{beam} \ln(t_{drill}) - C$, where D_p is the pore diameter, I is the electron beam current density, and A and C are constants (Figure 1a, gray dashed lines). At a beam intensity of 6.2 $\times$ 10^5 electrons/(nm^2·s), shrinking of the pore *via* EBID was observed at a rate of 7.5 nm/min in which amorphous carbon is drawn toward the beam allowing nanopores to be reproducibly formed with diameters of 1−25 nm. If desirable, it is possible to turn this material into crystalline material by employing graphene-promoting atomic rearrangement (*i.e.*, graphitization). This has been reported by low energy electron irradiation (<80 kV) or by annealing.[25,34]

Interestingly at 6.2 $\times$ 10^5 electrons/(nm^2·s) irradiation of the amorphous carbon shrinkage layer produced a structure known as graphitic polyhedral crystals (GPC), composed of curved graphitic connections between layers (Figure 2b).[29,35−37] These structures can be easily discriminated from the rest of the membrane since the amorphous region is slightly darker in the TEM images and the GPC structures have a concentric ring pattern (Figure 2d). The whole shrinkage layer does not turn into GPC, but instead, only the regions of the shrunk pore that had direct contact with the beam do (experiencing a current density of ~10^6 electrons/(nm^2·s)) which agrees with previous reports of graphitization by electron beam exposure (more images of GPC pores in Supporting Information, Figure S2).[38] Once the shrunk GPC pore is formed, it should be possible to graphitize the rest of the shrunk EBID layer by subsequent high temperature annealing in order to electrically connect the GPC to the surrounding graphene. However, since the pore surface is the key functional element of the sensor for ionic current measurements of DNA, we investigated the potential beneficial properties of the GPC nanopore edge. On the basis of the kinetic properties of electron beam sculpting, other structures were also fabricated including nanoribbons, nanometer scale cantilevers (both from existing graphene and from EBID processes), three-pronged nanogaps which could serve as source-drain-gate, and nanopore arrays (Figure S7).

To better characterize graphene thickness (*i.e.*, number of layers) and the graphene nanopore's edge structure, we performed TEM tomography during various stages of drilling and shrinking at 6.2 $\times$ 10^5 electrons/(nm^2·s); specifically after 20, 60, and 240 s producing pores of 8 nm, 25 nm, and 14 nm, respectively (Figure 3). On the basis of TEM tomography technique, we observed a thickness of the graphene-layers to be between 6 and 9 nm. With increasing beam exposure, the cross-sectional profile of the nanopore evolves over time. The initial profile is a double-cone structure mimicking that of TEM-drilled silicon nitride nanopores.[26] As the pore enlarges, the edges become more rounded; this likely due to the fact that the beam loses intensity as you travel further away from the beam center. Shrinking the pore produces an even rounder edge than the enlarged pore. These edges also are likely due to the spherically shaped layers of the GPC (tomography movies available in Supporting Information). The carbon growth and the formation of GPC were only observed laterally and no changes in the thickness of the membrane were observed. It can be concluded that the shrunk GPC-transformed pore, given its different atomic structure, is physically,[35] electrically,[39] and geometrically different when compared to the direct-beam fabrication method.

On the basis of pure ionic current measurements, several groups have investigated the ability to detect DNA using graphene nanopores experimentally[15−17] and using molecular simulations.[19,40,41] However, due

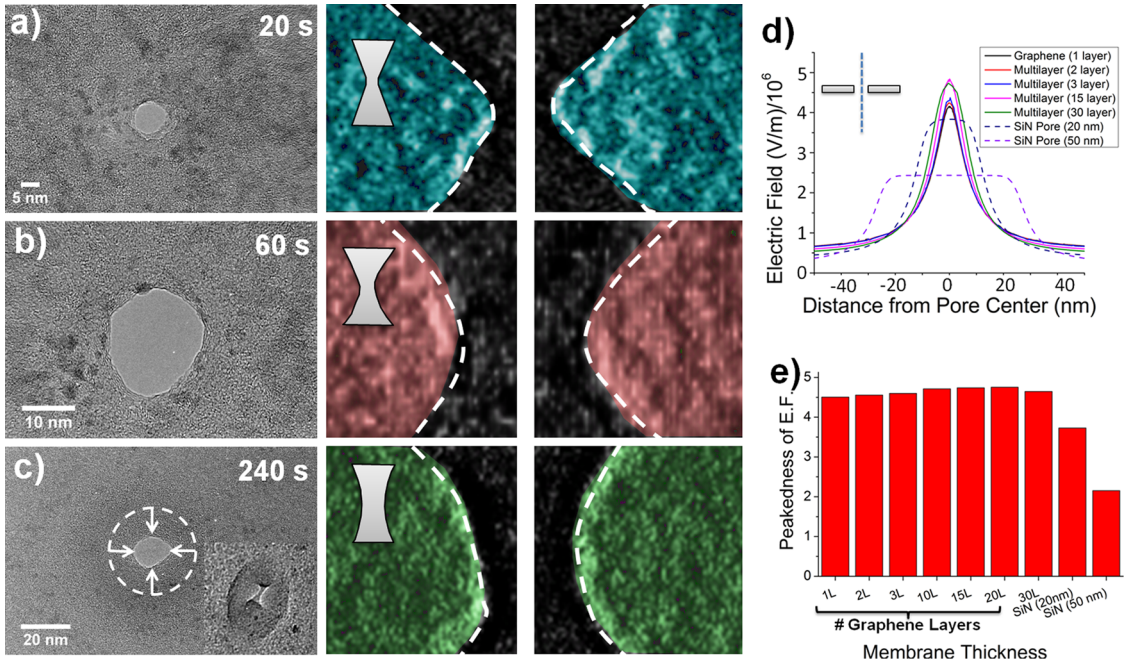

Figure 3. (a) TEM image and tomogram of a pore drilled at 6.2 × 10^5 electrons/(nm^2·s) and 20 s exposure time producing a pore ~8 nm in diameter. (b) A pore drilled at 6.2 × 10^5 electrons/(nm^2·s) with an exposure time of 60 s producing a pore ~25 nm in diameter. (c) A pore drilled at 6.2 × 10^5 electrons/(nm^2·s) with an exposure time of 240 s producing a shrunk pore with a diameter of ~14 nm (shrunk from an initial diameter of ~40 nm). Tomograms were obtained using a tilt series from −60 to +60 degrees using the SerialEM Software. (d) Electric field distribution along the axis of the pore with varying membrane thicknesses. (e) Statistical measure of the peakedness of the electric field distribution for various membrane thicknesses. Details of numerical simulations found in Supporting Information.

to the preferred use of single layer graphene for the above application, analysis on how the existence of multiple layers would affect the distribution of the electric field has not been investigated. Using numerical methods, the electric field distribution of single compared to multilayer graphene was actually found to be almost identical for a 10 nm pore (Figure 3d,e). Although the electric field generally becomes more focused with thinner membranes, we found that when the thickness of the pore (h) is smaller than the pore diameter (d), the effects of access resistance become more dominant. The increased contribution of access resistance can be shown quantitatively using the resistance expressions $R_{pore} = (\rho l/\pi r^2)$ and $R_{access} = (\rho/\pi r)$, where ρ is the solution resistivity, l is the length of the pore, and r is the radius of the pore. Using an arbitrary pore diameter of 2 nm, a 50 nm thick membrane has access resistance that is only 3.0% of the total resistance, whereas a membrane thickness of 0.3 nm yields a much larger access resistance contribution of 83.9%. Therefore, the benefits of decreasing the membrane thickness become negated as the aspect ratio of the pore decreases.

The length of the sensing zone of the pore is arguably measured by the peakedness of the electric field distribution along the axis of the pore. The main contributing factors for peakedness are the membrane thickness (*i.e.*, the length at which the electric field is nearly constant) and access resistance (*i.e.*, the falloff rate from the maximum electric field strength to the negligible electric field strengths found in the bulk solution). Using the statistical measure for peakedness (*i.e.*, kurtosis), it was found that the most peaked electric field distribution occurred at a membrane thickness of 5−6 nm (15−20 graphene sheets) for a 10 nm pore ($h_{optimal} = d/2$). Although the ideal pore diameter for sensing DNA is 2−3 nm, the ability to create such small pores is not an easy task and generally experiments are performed using much larger sized pores.[15−17] Since the number of layers, thickness and geometry of the graphene has such an imperative role in DNA−pore interactions and electric field distribution, multilayer graphene has promising applications to DNA sequencing and related analysis.

Detection of Long and Short DNA. The study of the interaction between graphene (both flat sheets and carbon nanotubes) with DNA bases has been of great interest recently due to the prospects of detecting DNA using graphene nanopores[15−17,19,40,42] and carbon nanotubes.[43−45] Several reports have suggested DNA bases are stabilized by π-stacking on the surface of graphene and carbon nanotubes.[40,43,44,46,47] These studies have shown that the interaction with the four types of nucleic acids is base dependent, but nevertheless, all DNA bases have been shown to interact significantly with the graphene surface.[44] Due to the physisorption nature of the interaction, the electronic properties of the base are not disturbed, allowing for

applications in DNA-sequencing *via* transverse conductance measurements.[15] The most interesting aspect of these interactions lies with their effects on DNA translocation kinetics through the pore. The work by Wells and colleagues[48] in particular have shown through Molecular Dynamics simulations that these interactions are critical to future DNA sequencing applications. Namely, since the interaction energy seems to be strongest with the graphene surface and not the edge, the DNA strand is expected to translocate in single nucleotide steps where the bases make quick transitions from one side of the single layer graphene nanopore to the other and thereby limiting the actual time spent within the pore. The second and perhaps most important aspect of these interactions is that the adhesion forces between exposed DNA bases and the graphene surface should reduce the translocation velocity of single stranded DNA as compared to double stranded DNA. For a comprehensive study of double stranded DNA translocating through a graphene nanopore using Molecular Dynamics, refer to work by Sathe and co-workers.[41] Both of these DNA-pore behaviors will be affected by the presence of GPC around the pore. With GPC nanopores, the graphene edge is replaced by a surface more comparable to that of graphene (*i.e.*, a slightly curved graphene surface). It is therefore expected that nanopores with a GPC edge can be used to slow down DNA translocations thereby alleviating one of the main issues with DNA sequencing applications of nanopores.[49]

DNA translocations were obtained with a nanopore having GPC-edges having a diameter of 5 nm. The conductance of the pore was 31 nS at 2 M KCl (Figure 4a) which is comparable to previous reports with multilayer pores at 1 M KCl (~13 nS).[17] DNA was introduced into one chamber of the flow cell producing transient drops in current corresponding to single DNA molecules. First, λ-DNA (48.5 kb, 5 nM) was used to characterize the pore producing events with characteristic event properties, namely, a uniform current drop and event durations described by an exponential (Figure 4c). The mean current drop value obtained in these experiments was 332 $\pm$ 62 pA as shown by the scatter plot in Figure 4b. Using a simple area of occlusion approximation given by A_{DNA}/A_p, the expected current drop for a 5 nm pore should be 19.4% (2.2 nm^2/5 nm^2) where as the experimental percent block was only 6.8% (332 pA/4900 pA). The smaller than expected percent block was also found by others[16] and may be caused by the low aspect ratio of graphene pores causing the sensing zone of the pore to extend outside the immediate region of the pore. The peak event duration was found to be 710 μs (250 mV driving voltage) which is longer than that reported by two independent studies which obtained translocation times of ~200 μs (100 and 160 mV driving voltage).[15,16] However, the translocation time was not as long as that reported by Schneider *et al.*,[17] which was 2.7 ms at an applied voltage of 200 mV. The distribution of residence times was also reported to be Gaussian instead of the falling exponential function found here (and previously reported as indicating strong DNA-pore interactions[11]) leading us to speculate different translocation kinetics all together.

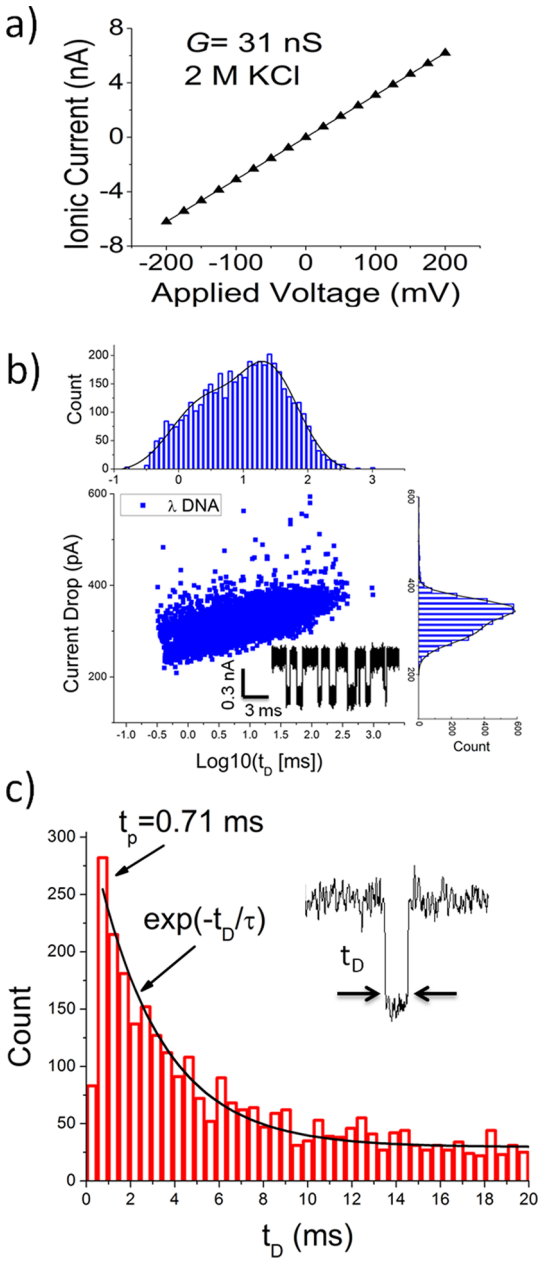

Figure 4. (a) Current *versus* voltage plot for a 5 nm multilayer graphene pore and 2 M KCl. (b) DNA translocation data for λ-DNA (5 nM concentration, 48.5 kb long) using a nanopore with a graphitic polyhedral edge. Current drop-translocation time scatter plot for double stranded λ-DNA at 250 mV (1 M KCl, 10 mM Tris, 1 M EDTA). (c) Histogram for the translocation time (t_D) showing an exponential dependence for $t_D > t_p$. Translocation events (n = 4388) were recorded at 1 M KCl, 10 mM Tris (pH 8), and 1 mM EDTA. The exponential curve fit parameter τ = 2.34 ms.

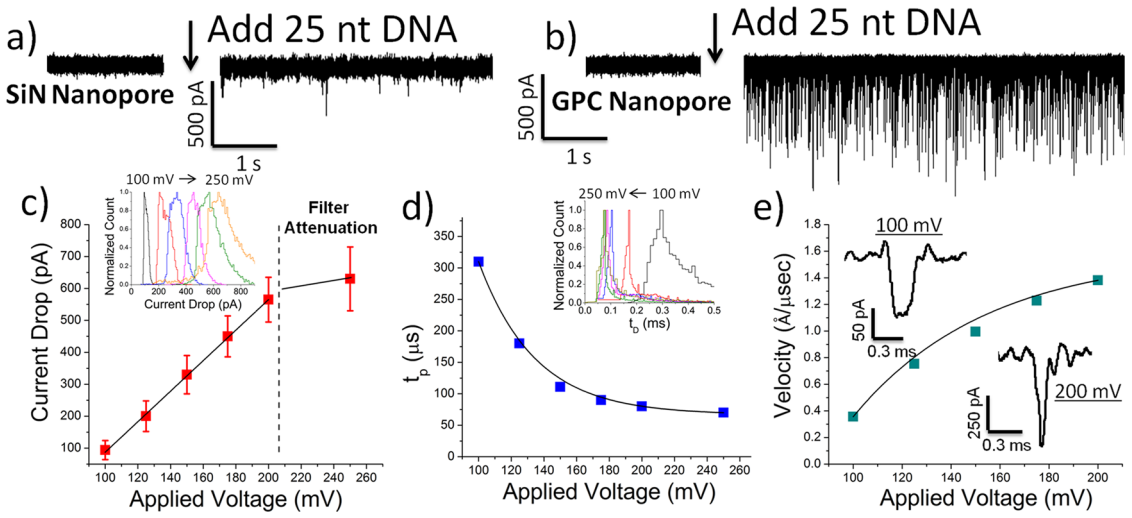

Figure 5. (a) Ionic current traces for single stranded DNA (25 bases in length) in a 50 nm thick silicon nitride nanopores (5 nm diameter). (b) Ionic current traces for a graphene nanopores with graphite polyhedral crystal (GPC) edges. (c) Current drop parameter, (d) peak translocation time (t_p), and (e) translocation velocity as a function of voltage. Events were recorded at 100 (n = 9458), 125 (n = 6854), 150 (n = 9616), 175 (n = 8624), 200 (n = 6932), and 250 mV (n = 8057) in 2 M KCl, 10 mM Tris (pH 8), 1 mM EDTA and 10 nM DNA.

To further investigate the benefit of DNA sensing and the dependence with single *versus* double stranded DNA, we also performed experiments with 25 nucleotide single stranded DNA. We observed that with silicon nitride nanopores there were fewer events and events that were detected were extremely short-lived (<50 μs). Also, the few number of events that were recorded had smaller than expected current drops (<1% conductance change from baseline) not consistent DNA suggesting attenuation of the events due to the low-pass filter. Using the same recording settings, the GPC pore could detect events more efficiently and with a peak translocation time that is well within the capability of the recording system; particularly at the 100 mV driving voltage. As expected, the current drop had a linear dependence with voltage and an exponential dependence for the event duration (Figure 5c,d) as was previously shown with silicon nitride pores within the voltage regime we test.[49,50] The smallest current drop value (94 $\pm$ 30 pA) was at 100 mV and could still be measured and analyzed. The linear increase in current drop is caused by higher current densities within the pore at higher voltages. However, as the current drop increases from 200 to 250 mV, the larger current change as well as the shorter duration of the events make the events attenuated by the filter (Figure 5c). The current drop still increases between 200 and 250 mV; however, at 250 mV, the current drop deviates from the linear relationship which exists at the lower voltages.

Due to the energy barrier that exists at the entrance of the pore, translocation time follows an exponential dependence. Other models have used a force balance between the electric force and the viscous drag across the whole molecule yielding an inverse relationship;[49] however, that was not the best fit for this data. It should be emphasized that the single stranded DNA traversed the pore even more slowly than the double stranded λ-DNA which is likely due to the bases interacting with the graphene surface. Due to contributions of access resistance of similar length-scale pores, the translocation velocity was calculated using the corrected velocity equation used by Meller *et al.*:[50] $v_{DNA} = (L_{DNA} + 0.35L_{pore})/t_p$ where t_p is the peak translocation time of the histograms shown in Figure 5b. It should be noted that the velocity of the 25 nucleotide-long DNA fragment in our pores (0.35 Å/μs at 100 mV and room temperature) is much slower than the velocity of 3000 bp DNA in SiN pores (125 Å/μs at 120 mV),[51] 6557 bp DNA in silicon-oxide nanopores (146 Å/μs at 120 mV)[52] and of the same order of magnitude for α-hemolysin with 25 nucleotide-long ss-DNA at 2 °C (0.16 Å/μs at 120 mV).[50] At 100 mV, we obtained a single base residence time of 12.4 μs, which is the slowest velocity reported at room temperature using a solid-state nanopore.

The slowing down of DNA while inside the pore is not a novel idea and has been the focus of much research. One of the earliest methods of slowing down the translocation process was using solutions of increased viscosity.[49] In this experiment, they used a 4−8 nm silicon nitride pore with varying concentrations of glycerol and obtained a velocity of approximately 9 Å/μs. Other techniques include using a pore smaller than the diameter of double stranded DNA[53] as well as optically trapping a dielectric bead attached to a DNA molecule and controlling the speed independently. The last experiment seems the most robust but lacks the high-throughput sensing required for next generation DNA sequencing. Instead, the study focused on the measurement of forces on the DNA

molecule while inside the pore. The most recent work by the same group also used lithium chloride instead of potassium chloride as the bulk electrolyte.[54] Due to the lithium binding more strongly to the DNA, they were able to achieve slower translocation rates. Viscosity and electrolyte type could potentially be used in conjunction with material properties to further slow down DNA in a graphene pore to achieve the translocation rates needed for DNA sequencing.

CONCLUSIONS

In terms of DNA sequencing, graphene nanopores have been reported to offer two main advantages including: (1) an atomically thin membrane which allows for finer single-molecule resolution and (2) graphene can potentially measure DNA's transverse conductance (thereby obtaining its sequence) as well as control its motion through the pore. Multilayer graphene have also been reported to provide more flexibility in tailoring the electronic properties of graphene; offering more options to meet device specifications.[28] Without the presence of GPC around the nanopore edge, multilayer graphene is still useful for conductance measurements of DNA bases since each graphene layer conducts only in-plane.[15] Despite a seemingly strong preference for single-layer graphene, multilayer graphene may actually provide the most information about DNA by measuring from each base individually but several times as it translocates the pore. Alternatively, due to the flexible nature of single stranded DNA, multilayer graphene can further ensure the measurement of a single base by restricting the bases movement.

In the future, prospective DNA sequencing technologies must overcome some major challenges in order to resolve single base identity. One criterion for future devices is that the device should read the sequence without digesting the DNA into smaller pieces since this process increases the complexity of the analysis and lowers throughput. In the case of single strand sequencing using nanopores, gaining confidence of base identity can be achieved by increasing the residence time inside the pore. For optical detection schemes, localizing the source of the light down to the nano- or even subnanoscale is the major challenge. At the current state of technology, manipulating the movement of DNA may be more feasible compared to complex and costly optical detection schemes. Other techniques to manipulate single stranded DNA including atomic force microscopy (AFM) and optical tweezers are not easy or high throughput. The prospect of using material properties to control and manipulate DNA through interaction forces is tempting because of its ability to do so in a high-throughput manner.

In summary, we report on the beam intensity-dependent nature of pore drilling and demonstrate that selection of spot size should be based on the desired pore diameter in order to minimize edge defects. More interestingly, we observed the ability to sculpt multilayer graphene using lower than conventional current densities which yielded the unique formation of graphitic polyhedral crystals around the nanopore edge. We also propose that multilayer graphene, particularly the growth of graphite polyhedral crystals, may provide some unique advantages for future DNA sequencing applications such as slowing the DNA molecule while translocating the pore through favorable interactions with the pore wall. We provide evidence for this hypothesis by detecting both single and double stranded DNA and showing that the single stranded DNA (25 bases long) travels through the pore significantly slower than traditional experiments with silicon nitride nanopores.

MATERIALS AND METHODS

Fabrication. A majority of drilling kinetics, as well as tomography, were performed by transferring graphene to a holey carbon TEM grid. Almost all holes in the holey carbon had a suspended sheet of graphene allowing drilling to be performed repeatedly on the same TEM sample.To make nanopores capable of electrochemical studies, graphene was transferred to various sized silicon nitride pores ranging in size from 200 to 1500 nm in diameter. Silicon nitride nanopores were drilled in a 50 nm thick free-standing silicon nitride membrane which was supported on all sides by a silicon chip (5.5 $\times$ 5.5 mm^2). Fabrication of this membrane consisted of first depositing a layer of low-stress silicon nitride on a silicon wafer using low pressure chemical vapor deposition (LPCVD) followed by photolithography, deep reactive ion etching (DRIE) and KOH etching to form a 50 $\times$ 50 μm^2 square membrane. Pores were then drilled using a focused ion beam (FIB, FEI Strata DB235). The TEM used for all drilling experiments was a JEOL JEM 2100 equipped with a LaB_6 electron source.

We used a graphene transfer process similar to that reported by Garaj *et al.*[15] Briefly, graphene was grown by CVD on a copper substrate followed by spin coating a polymer (PMMA) on the surface.[15] The copper substrate was then etched using ferric chloride thereby releasing the graphene. A new support (silicon nitride chip or carbon grid) was then used to scoop up the floating graphene/PMMA. PMMA was then removed using thorough solvent washes including a 30 min soak in heated acetone.

Tomography. Tomography was performed using a high tilt tomography holder capable of -60 to 60° tilting. The tilt series was accomplished using SerialEM, and reconstructed using IMOD and Chimera.

Single Channel Recordings. Pore characterization and event recording were accomplished by placing the nanopore between two electrolytic half cells filled with buffered potassium chloride. The nanopore chip was held in place using a custom built polycarbonate flow cell with PDMS gaskets to ensure that the only path of ionic current is through the nanopore. Electrodes (Ag/AgCl) were placed in both chambers and connected to the headstage of a patch clamp amplifier (Axopatch 200B, Molecular Devices, Inc.) which allowed the ionic current to be measured at various applied voltages. Signals were recorded at 250 kHz with a low-pass Bessel filter of 2, 5, and 10 kHz. λ-DNA (48.5 kb) was added at a concentration of 5 nM to the cis chamber of the flow cell which led to transient decreases in current corresponding to the translocation of individual DNA

molecules. Primer DNA (single stranded with the following sequence: CCCTGCGTGAAGGCCACCCCCCTGT) was also translocated through the pore following the same procedure but at a range of voltages.

Conflict of Interest: The authors declare no competing financial interest.

Supporting Information Available: Long-term exposure kinetics, additional images of TEM-drilled pores, diffraction patterns of polycrystalline graphene which was avoided when drilling, one additional tomogram, numerical simulations of the electric field distribution around the graphene pore, ion permeability calculations for a graphene pore, and additional TEM images of fabricated nanostructures. This material is available free of charge *via* the Internet at http://pubs.acs.org.

Acknowledgment. This material is based upon work supported by the National Science Foundation Graduate Research Fellowship under Grant ID No. 2010095296 and the HFSP young investigator award (RGY0075/2009-C). C.W.A. would also like to acknowledge the financial support from MEST (2011-0032147) and MKE(A004600091). The authors would like to especially thank Anmiv Prabhu and Gaurav Goyal for help with drilling the silicon nitride nanopores used as support structures for the graphene. Also a special thanks to the Centralized Research Facility at Drexel University for use of their equipment and Craig Johnson, Yuri Gogotsi, and Joseph Robertson for helpful discussions.

REFERENCES AND NOTES

1. Oukhaled, A.; Cressiot, B.; Bacri, L.; Pastoriza-Gallego, M.; Betton, J.-M.; Bourhis, E.; Jede, R.; Gierak, J.; Auvray, L.; Pelta, J. Dynamics of Completely Unfolded and Native Proteins through Solid-State Nanopores as a Function of Electric Driving Force. *ACS Nano* **2011**, *5*, 3628–3638.
2. Dekker, C. Solid-State Nanopores. *Nat. Nano* **2007**, *2*, 209–215.
3. Iqbal, S. M.; Akin, D.; Bashir, R. Solid-State Nanopore Channels with DNA Selectivity. *Nat. Nano* **2007**, *2*, 243–248.
4. Sauer-Budge, A. F.; Nyamwanda, J. A.; Lubensky, D. K.; Branton, D. Unzipping Kinetics of Double-Stranded DNA in a Nanopore. *Phys. Rev. Lett.* **2003**, *90*, 238101.
5. Freedman, K. J.; Jürgens, M.; Prabhu, A.; Ahn, C. W.; Jemth, P.; Edel, J. B.; Kim, M. J. Chemical, Thermal, and Electric Field Induced Unfolding of Single Protein Molecules Studied Using Nanopores. *Anal. Chem.* **2011**, *83*, 5137–5144.
6. Kasianowicz, J.; Brandin, E.; Branton, D.; Deamer, D. Characterization of Individual Polynucleotide Molecules Using a Membrane Channel. *P. Natl. Acad. Sci.* **1996**, *93*, 13770–13773.
7. Freedman, K. J.; Bastian, A. R.; Chaiken, I.; Kim, M. J. Solid-State Nanopore Detection of Protein Complexes: Applications in Healthcare and Protein Kinetics. *Small* **2013**, *9*, 750–759.
8. Madampage, C.; Andrievskaia, O.; Lee, J. Nanopore Detection of Antibody Prion Interactions. *Anal. Biochem.* **2010**, *396*, 36–41.
9. Hornblower, B.; Coombs, A.; Whitaker, R. D.; Kolomeisky, A.; Picone, S. J.; Meller, A.; Akeson, M. Single-Molecule Analysis of DNA-Protein Complexes Using Nanopores. *Nat. Methods* **2007**, *4*, 315–317.
10. Keyser, U. F.; Koeleman, B. N.; van Dorp, S.; Krapf, D.; Smeets, R. M. M.; Lemay, S. G.; Dekker, N. H.; Dekker, C. Direct Force Measurements on DNA in a Solid-State Nanopore. *Nat. Phys.* **2006**, *2*, 473–477.
11. Wanunu, M.; Sutin, J.; McNally, B.; Chow, A.; Meller, A. DNA Translocation Governed by Interactions with Solid-State Nanopores. *Biophys. J.* **2008**, *95*, 4716–4725.
12. Talaga, D. S.; Li, J. Single-Molecule Protein Unfolding in Solid State Nanopores. *J. Am. Chem. Soc.* **2009**, *131*, 9287–9297.
13. Kowalczyk, S. W.; Tuijtel, M. W.; Donkers, S. P.; Dekker, C. Unraveling Single-Stranded DNA in a Solid-State Nanopore. *Nano Lett.* **2010**, *10*, 1414–1420.
14. Wanunu, M.; Dadosh, T.; Ray, V.; Jin, J.; McReynolds, L.; Drndic, M. Rapid Electronic Detection of Probe-Specific MicroRNAs using Thin Nanopore Sensors. *Nat. Nano* **2010**, *5*, 807–814.
15. Garaj, S.; Hubbard, W.; Reina, A.; Kong, J.; Branton, D.; Golovchenko, J. Graphene as a Subnanometre Trans-Electrode Membrane. *Nature* **2010**, *467*, 190–193.
16. Merchant, C. A.; Healy, K.; Wanunu, M.; Ray, V.; Peterman, N.; Bartel, J.; Fischbein, M. D.; Venta, K.; Luo, Z.; Johnson, A. C.; *et al.* DNA Translocation through Graphene Nanopores. *Nano Lett.* **2010**, *10*, 2915–2921.
17. Schneider, G.; Kowalczyk, S. W.; Calado, V. E.; Pandraud, G. g.; Zandbergen, H. W.; Vandersypen, L. M.; Dekker, C. DNA Translocation through Graphene Nanopores. *Nano Lett.* **2010**, *10*, 3163–3167.
18. Rasuli, R.; Ahadian, M. Mechanical Properties of Graphene Cantilever from Atomic Force Microscopy and Density Functional Theory. *Nanotechnology* **2010**, *21*, 185503.
19. He, Y.; Scheicher, R.; Grigoriev, A.; Ahuja, R.; Long, S.; Huo, Z.; Liu, M. Enhanced DNA Sequencing Performance through Edge Hydrogenation of Graphene Electrodes. *Adv. Funct. Mater.* **2011**, *21*, 2674–2679.
20. Fischbein, M.; Drndić, M. Electron Beam Nanosculpting of Suspended Graphene Sheets. *App. Phys. Lett.* **2008**, *93*, 113107.
21. Meyer, J.; Kisielowski, C.; Erni, R.; Rossell, M.; Crommie, M.; Zettl, A. Direct Imaging of Lattice Atoms and Topological Defects in Graphene Membranes. *Nano Lett.* **2008**, *8*, 3582–3586.
22. Banhart, F. The Formation of a Connection between Carbon Nanotubes in an Electron Beam. *Nano Lett.* **2001**, *1*, 329–332.
23. Hass, J.; Feng, R.; Li, T.; Li, X.; Zong, Z.; De Heer, W.; First, P.; Conrad, E.; Jeffrey, C.; Berger, C. Highly Ordered Graphene for Two Dimensional Electronics. *Appl. Phys. Lett.* **2006**, *89*, 1431061–1431063.
24. Wang, M.; Wang, J.; Chen, Q.; Peng, L. Fabrication and Electrical and Mechanical Properties of Carbon Nanotube Interconnections. *Adv. Funct. Mater.* **2005**, *15*, 1825–1831.
25. Yasuda, A.; Kawase, N.; Banhart, F.; Mizutani, W.; Shimizu, T.; Tokumoto, H. Graphitization Mechanism during the Carbon-Nanotube Formation Based on the *in Situ* HRTEM Observation. *J. Phys. Chem. B* **2002**, *106*, 1849–1852.
26. Kim, M.; Wanunu, M.; Bell, D.; Meller, A. Rapid Fabrication of Uniformly Sized Nanopores and Nanopore Arrays for Parallel DNA Analysis. *Adv. Mater.* **2006**, *18*, 3149–3153.
27. Heng, J.; Ho, C.; Kim, T.; Timp, R.; Aksimentiev, A.; Grinkova, Y.; Sligar, S.; Schulten, K.; Timp, G. Sizing DNA using a Nanometer-Diameter Pore. *Biophys. J.* **2004**, *87*, 2905–2911.
28. Nilsson, J.; Neto, A.; Guinea, F.; Peres, N. Electronic Properties of Graphene Multilayers. *Phys. Rev. Lett.* **2006**, *97*, 266801.
29. Rotkin, S.; Gogotsi, Y. Analysis of Non-Planar Graphitic Structures: From Arched Edge Planes of Graphite Crystals to Nanotubes. *Mater. Res. Innovations* **2002**, *5*, 191–200.
30. Girit, Ç.; Meyer, J.; Erni, R.; Rossell, M.; Kisielowski, C.; Yang, L.; Park, C.; Crommie, M.; Cohen, M.; Louie, S. Graphene at the Edge: Stability and Dynamics. *Science* **2009**, *323*, 1705–1708.
31. Song, B.; Schneider, G. g. F.; Xu, Q.; Pandraud, G. g.; Dekker, C.; Zandbergen, H. Atomic-Scale Electron-Beam Sculpting of Near-Defect-Free Graphene Nanostructures. *Nano Lett.* **2011**, *11*, 2247–2250.
32. Ferrari, A. C.; Meyer, J. C.; Scardaci, V.; Casiraghi, C.; Lazzeri, M.; Mauri, F.; Piscanec, S.; Jiang, D.; Novoselov, K. S.; Roth, S.; *et al.* Raman Spectrum of Graphene and Graphene Layers. *Phys. Rev. Lett.* **2006**, *97*, 187401.
33. Teweldebrhan, D.; Balandin, A. A. Modification of Graphene Properties due to Electron-Beam Irradiation. *App. Phys. Lett.* **2009**, *94*, 013101–013103.
34. Ugarte, D. Curling and Closure of Graphitic Networks under Electron-Beam Irradiation. *Nature* **1992**, *359*, 707–709.
35. Gogotsi, Y.; Libera, J. A.; Kalashnikov, N.; Yoshimura, M. Graphite Polyhedral Crystals. *Science* **2000**, *290*, 317–320.

36. Okuno, H.; Palnichenko, A.; Despres, J. F.; Issi, J. P.; Charlier, J. C. Synthesis of Graphite Polyhedral Crystals using a Combustion Flame Method. *Carbon* **2005**, *43*, 692–697.
37. Gogotsi, Y.; Dimovski, S.; Libera, J. A. Conical Crystals of Graphite. *Carbon* **2002**, *40*, 2263–2267.
38. Duan, H.; Xie, E.; Han, L.; Xu, Z. Turning PMMA Nanofibers into Graphene Nanoribbons by *in Situ* Electron Beam Irradiation. *Adv. Mater.* **2008**, *20*, 3284–3288.
39. Andersson, O. E.; Prasad, B. L. V.; Sato, H.; Enoki, T.; Hishiyama, Y.; Kaburagi, Y.; Yoshikawa, M.; Bandow, S. Structure and Electronic Properties of Graphite Nanoparticles. *Phys. Rev. B* **1998**, *58*, 16387–16395.
40. Nelson, T.; Zhang, B.; Prezhdo, O. V. Detection of Nucleic Acids with Graphene Nanopores: *Ab Initio* Characterization of a Novel Sequencing Device. *Nano Lett.* **2010**, *10*, 3237–3242.
41. Sathe, C.; Zou, X.; Leburton, J.-P.; Schulten, K. Computational Investigation of DNA Detection Using Graphene Nanopores. *ACS Nano* **2011**, *5*, 8842–8851.
42. Postma, H. W. Rapid Sequencing of Individual DNA Molecules in Graphene Nanogaps. *Nano Lett.* **2010**, *10*, 420–425.
43. Gigliotti, B.; Sakizzie, B.; Bethune, D.; Shelby, R.; Cha, J. Sequence-Independent Helical Wrapping of Single-Walled Carbon Nanotubes by Long Genomic DNA. *Nano Lett.* **2006**, *6*, 159–164.
44. Meng, S.; Maragakis, P.; Papaloukas, C.; Kaxiras, E. DNA Nucleoside Interaction and Identification with Carbon Nanotubes. *Nano Lett.* **2007**, *7*, 45–50.
45. Staii, C.; Johnson, A., Jr.; Chen, M.; Gelperin, A. DNA-Decorated Carbon Nanotubes for Chemical Sensing. *Nano Lett.* **2005**, *5*, 1774–1778.
46. Antony, J.; Grimme, S. Structures and Interaction Energies of Stacked Graphene−Nucleobase Complexes. *Phys. Chem. Chem. Phys.* **2008**, *10*, 2722–2729.
47. Gowtham, S.; Scheicher, R.; Ahuja, R.; Pandey, R.; Karna, S. Physisorption of Nucleobases on Graphene: Density-Functional Calculations. *Phys. Rev. B: Condens. Matter* **2007**, *76*, 033401.
48. Wells, D. B.; Belkin, M.; Comer, J.; Aksimentiev, A. Assessing Graphene Nanopores for Sequencing DNA. *Nano Lett.* **2012**, *12*, 4117–4123.
49. Fologea, D.; Uplinger, J.; Thomas, B.; McNabb, D.; Li, J. Slowing DNA Translocation in a Solid-State Nanopore. *Nano Lett.* **2005**, *5*, 1734–1737.
50. Meller, A.; Nivon, L.; Branton, D. Voltage-Driven DNA Translocations through a Nanopore. *Phys. Rev. Lett.* **2001**, *86*, 3435–3438.
51. Li, J.; Gershow, M.; Stein, D.; Brandin, E.; Golovchenko, J. A. DNA Molecules and Configurations in a Solid-State Nanopore Microscope. *Nat. Mater.* **2003**, *2*, 611–615.
52. Storm, A. J.; Storm, C.; Chen, J.; Zandbergen, H.; Joanny, J.-F.; Dekker, C. Fast DNA Translocation through a Solid-State Nanopore. *Nano Lett.* **2005**, *5*, 1193–1197.
53. Mirsaidov, U.; Comer, J.; Dimitrov, V.; Aksimentiev, A.; Timp, G. Slowing the Translocation of Double-Stranded DNA Using a Nanopore Smaller than the Double Helix. *Nanotechnology* **2010**, *21*, 395501.
54. Kowalczyk, S. W.; Wells, D. B.; Aksimentiev, A.; Dekker, C. Slowing Down DNA Translocation through a Nanopore in Lithium Chloride. *Nano Lett.* **2012**, *12*, 1038–1044.